Axisymmetric Granular Collapse: A Transient 3D Flow Test of Viscoplasticity

Laurent Lacaze* and Rich R. Kerswell†

Department of Mathematics, University Walk, Bristol University, Bristol BS8 1TW, United Kingdom

(Received 26 August 2008; published 13 March 2009)

A viscoplastic continuum theory has recently been proposed to model dense, cohesionless granular flows [P. Jop *et al.*, Nature (London) **441**, 727 (2006)]. We confront this theory for the first time with a transient, three-dimensional flow situation—the simple collapse of a cylinder of granular matter onto a horizontal plane—by extracting stress and strain rate tensors directly from soft particle simulations. These simulations faithfully reproduce the different flow regimes and capture the observed scaling laws for the final deposit. Remarkably, the theoretical hypothesis that there is a simple stress-strain rate tensorial relationship does seem to hold across the whole flow even close to the rough boundary provided the flow is dense enough. These encouraging results suggest viscoplastic theory is more generally applicable to transient, multidirectional, dense flows and open the way for quantitative predictions in real applications.

DOI: 10.1103/PhysRevLett.102.108305 PACS numbers: 47.57.Gc, 47.57.Qk

A predictive theory for the flow of granular media remains a major objective for the physics community with industrial facilities handling granular materials operating well below design efficiency and destructive natural phenomena such as snow avalanches, landslides and debris flows difficult to safeguard against [1,2]. A central difficulty is that the behavior of granular materials is not easily classified as being either solid, liquid or gaslike with multiple phases sometimes appearing simultaneously. In particular, the solid-liquid regime where there is a dense granular flow coexisting with a stopped solidlike deposit remains a considerable modelling challenge. In industrial (e.g., silo flow) and geophysical (e.g., avalanches) applications, the size of the constituent particles ($\gg \mu$m) means that thermal effects are completely negligible compared to external forces such as gravity [1]. The dynamics are then dominated by the inelastic collisions between particles which involve highly nonlinear frictional forces. As a further complication, there is typically no scale separation between the microscopic (granular) dimension and the length scales over which the flow varies. Notwithstanding this, a viscoplastic continuum theory is starting to emerge [3] for dense granular media built upon the observations that a nonzero shear rate is needed to initiate movement and, once moving, there is a complicated flow dependence on the shear rate. At the heart of this theory is a dimensionless inertial number, I which is a *local* ratio of a macroscopic deformation time scale to an inertial time scale [4]. Numerical simulations of a simple sheared cell [5,6] had identified the importance of this quantity which was subsequently realized to be also highly relevant to other flows with a single shear plane [7]. Jop *et al.* [3] then provided a multidimensional generalization by defining $I := |\dot{\gamma}|d/\sqrt{P/\rho}$ and tensorializing the stress-strain relationship to

$$\tau_{ij} = \eta \dot{\gamma}_{ij}, \quad \text{with} \quad \eta := \mu(I)P/|\dot{\gamma}|, \tag{1}$$

where P is the isotropic pressure, $|\dot{\gamma}| := \sqrt{\frac{1}{2}\dot{\gamma}_{ij}\dot{\gamma}_{ij}}$ is the second invariant of the strain rate tensor $\dot{\gamma}_{ij} := u_{i,j} + u_{j,i}$, $u_{i,j}$ is the jth derivative of the ith velocity component, d is the particle diameter, ρ is the particle density, $\tau_{ij} := \sigma_{ij} + P\delta_{ij}$ is the deviatoric stress tensor (σ_{ij} being the stress tensor), η is the viscosity and μ a friction coefficient. By solving the continuum equations with the rheology (1), Jop *et al.* achieved predictions within 15% of actual flow velocities for a steady, unidirectional granular flow sheared in both cross-stream directions.

In this Letter, we confront this new theory with a transient three-dimensional situation where the flow is not unidirectional to test its applicability to real flows of practical interest. The flow situation studied is the intriguingly simple tabletop flow generated by a collapsing granular cylindrical column [8,9]. This is a particularly good test case because the initial condition is well defined, the subsequent dynamics are rich, combining a number of different flow regimes, and the flow duration is short enough that realistic discrete element simulations (DEM) can be done to calculate the stress and strain rates everywhere at any given time.

The collapsing column experiment consists of releasing a stationary cylinder of granules so that they fall and spread out on a horizontal surface. If the aspect ratio $a := h_0/r_0$ (h_0 and r_0 being the height and radius of the initial cylinder) of the column is small ($\lesssim 2$), the collapse starts at the column edge and propagates inwards either stopping before the top is totally eroded away (so the final maximum height $h_\infty = h_0$) or eventually leading to a complete collapse ($h_\infty < h_0$). If $a \gtrsim 2$, the column collapses instantaneously as a whole with three flow phases evident: (i), the free-fall regime where the top of the cylinder falls ballistically; (ii), a heap regime where moving grains flow over a growing inclined stationary deposit; and (iii), shallow layer regime where the motion is dominantly horizontal. Simple

power laws exist for the runout, $(r_\infty - r_0)/r_0 \sim a^{1/2}$ [8,9], and maximum height $h_\infty/h_0 \sim a^{-1}$ [8] or $\sim a^{-5/6}$ [9] of the final deposit (see Fig. 1) with only the numerical prefactors appearing material-dependent [10]. The observation $h_\infty \sim h_0/a = r_0$ is particularly striking as this implies that the final height becomes *independent* of the initial height for a sufficiently tall starting column. Efforts to explain these scalings have either concentrated on shallow layer modeling [11–13] or two-dimensional DEM (hard [14,15] and soft [16] particle).

Measuring pointwise stress and strain rates for this flow in the laboratory is impractical so three-dimensional DEM was carried out [17]. Up to 2×10^5 monodisperse, cohesionless, frictional, inelastic spheres of $d = 2$ mm diameter randomly packed into cylinders with aspect ratio $a \in [0.5, 20]$ were released over a roughened horizontal plane on which a monolayer of the same spheres was glued. The code used a Hertz-Mindlin theory to model the contact physics of colliding (soft) spheres (see [18] for details). The results were insensitive (see [15,18]) to the coefficient of restitution e provided e is not too close to 1 so this was taken nominally as 0.5 whereas the coefficient of (microscopic) friction μ_m was varied. Calculations were mainly performed with initial radii of $r_0 = 2$ cm or 3.5 cm implying a "granularity" of 10 or 17.5 spheres, respectively, across a radius compared to $\gtrsim 50$ in experiments. Figure 1 shows that the DEM captures the same scaling laws as seen in experiments, with the $r_0 = 3.5$ cm data having a slightly larger runout prefactor than the $r_0 = 2$ cm data. This discrepancy is well within the experimental data spread but is significant compared to the variability of repeated "identical" numerical experiments (the columns were filled by randomly dropping granules from a fixed height). Two tests for larger values of r_0 ($r_0 = 6$ cm, $a = 1$ and $r_0 = 7.5$ cm, $a = 0.5$), however, reproduced the $r_0 = 3.5$ cm runout data, indicating that, at least for small a, the effects of granularity on the collapse are lost within the numerical error bars at this r_0. Figure 2 shows a typical collapse for $a = 5$ calculated using DEM. An intermediate flow state is characterized by its upper moving free surface and the lower static interface which delineates the growing deposit. The three phases of the flow are illustrated in Fig. 3, where the free-fall regime (i) is characterized by growing vertical kinetic energy, the heap-flow regime (ii) by the conversion of vertical to radial kinetic energy and the shallow layer regime (iii) by the gradual decline of the dominant radial kinetic energy.

The viscoplastic hypothesis (1) is made under the assumption that the volume fraction is constant in the limit of dense flows. As stress and strain rate tensors are extracted directly from the collapsing compressible flow data [19], we actually worked with the equivalent expression

$$\tau_{ij} = \eta \dot{\gamma}^c_{ij} \quad \text{where } \dot{\gamma}^c_{ij} := \dot{\gamma}_{ij} - \tfrac{1}{3}\dot{\gamma}_{ii}\delta_{ij} \qquad (2)$$

is simply the nonisotropic part of the rate-of-strain tensor. To test this modified hypothesis (2), $\boldsymbol{\tau}$ and $\dot{\boldsymbol{\gamma}}^c$ were calculated over the flow domain at 5 to 10 different times during a collapse and over collapses of various different aspect

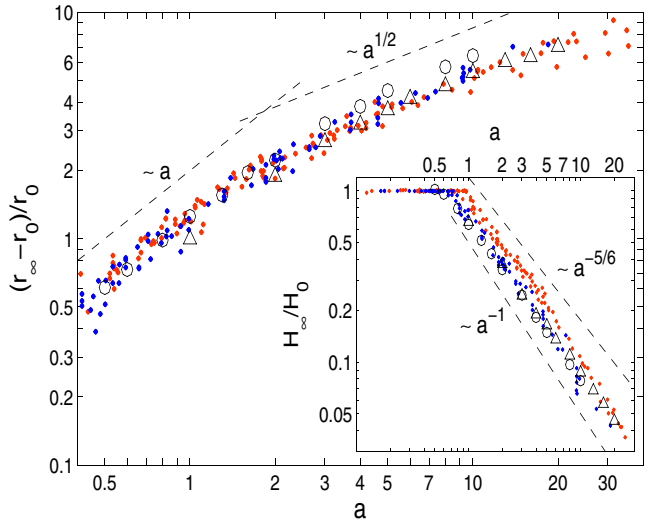

FIG. 1 (color online). Discrete element simulations and experimental data of the nondimensional runout $(r_\infty - r_0)/r_0$ and maximum final height (inset) as a function of a. Open symbols correspond to numerical results for $d = 2$ mm, $r_0 = 2$ cm (△) and $r_0 = 3.5$ cm (○) ($\mu_m = 0.5$) and dots are experimental results: data from Lajeunesse *et al.* [8] (dark/blue) and from Lube *et al.* [9] (light/red). ([8] claims $h_\infty/h_0 \sim a^{-1}$ whereas [9] quote $\sim a^{-5/6}$.) The symbol size of the numerical data indicates the variability over repeated runs.

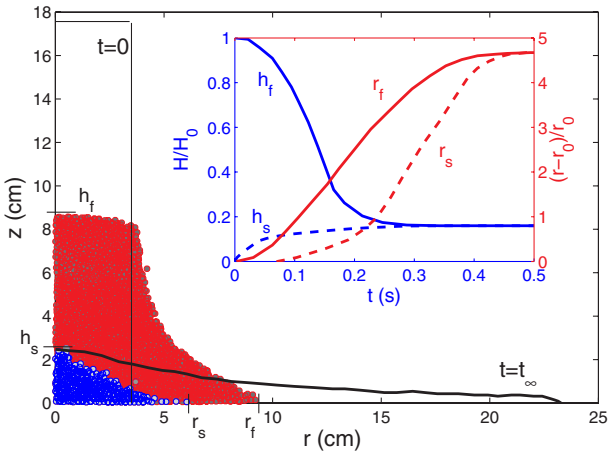

FIG. 2 (color online). Granular pile and static interface evolution as a function of time in the (r, z) plane ($a = 5$, $r_0 = 3.5$ cm, $\mu_m = 0.5$) from DEM. Thick line corresponds to the final deposit and the thin line is the initial configuration. An intermediate profile is also shown at $t = 0.14$ s to illustrate the growing stationary deposit (dark/blue; height h_s, radius r_s) and the flowing dense layer (light/red; height h_f, radius r_f). The inset shows how these two heights and radii evolve over time (normalized using the initial height H_0 and radius r_0).

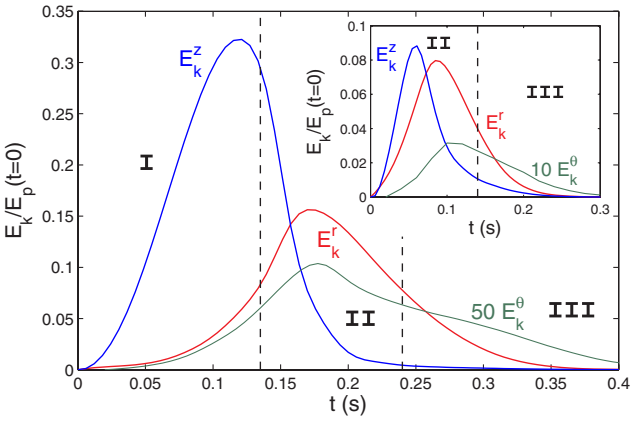

FIG. 3 (color online). Evolution of the radial kinetic energy E_k^r (red), azimuthal kinetic energy E_k^θ (green) and vertical kinetic energy E_k^z (blue) where $E_k^\alpha := \Sigma_{n=1}^{N} \frac{1}{2} m u_{\alpha,n}^2$, $u_{\alpha,n}$ is the velocity of the nth particle in the α ($= r$, θ or z) direction for the run of Fig. 2. N is the total number of particles, m is the mass of each particle and g is gravity. *Inset*: same quantities but for $a = 1$ where there is no free-fall regime I. [All quantities have been nondimensionalized by the initial potential energy $E_p(t = 0)$].

ratios. These were calculated using a standard coarse-graining approach (Eq. 5, [20]) using a step function weighting. Averages were calculated over tori around the axis of symmetry with a $3d \times 3d$ square cross-section in the (r, z) plane. This was possible because the flow is axisymmetric to a large degree ($E_k^\theta \ll E_k^z, E_k^r$, see Fig. 3) and meant that a significant number of particles contributed to the average at any one time. For a typical snapshot of the flow, data were calculated at ≈ 500 points in a (r, z) grid (see Fig. 4) determined by ensuring a 50% overlap between neighboring $3d \times 3d$ boxes.

To test how close $\boldsymbol{\tau}$ and $\dot{\boldsymbol{\gamma}}^c$ were to being simple multiples of each other, two estimators of η were used: $|\tau|/|\dot{\gamma}^c|$ where $|\tau| = \sqrt{\frac{1}{2}\tau_{ij}\tau_{ij}}$ is the second invariant (similarly for $\dot{\gamma}^c$), and the ratio of the maximum shear component $\tau_{\hat{r}\hat{z}}$ to $\dot{\gamma}^c_{\hat{r}\hat{z}}$ where $\hat{r}$ and $\hat{z}$ are the appropriately transformed coordinates (finding the orientation of the maximum shear was a good but not infallible way to predict the local flow direction). Only data for which the pressure exceeded 5% of the maximum were used to exclude the initial free-fall regime high in the column where the grains are not in frictional contact with each other (see Fig. 4). Of the data points which remained, the principal axes of $\boldsymbol{\tau}$ and $\dot{\boldsymbol{\gamma}}^c$ were surprisingly well-aligned, 95% to within 10°. The misalignment that does occur is invariably at the low-density free surface and near low-speed regions (the axis of symmetry and the static-to-flowing interface): see Fig. 4. No

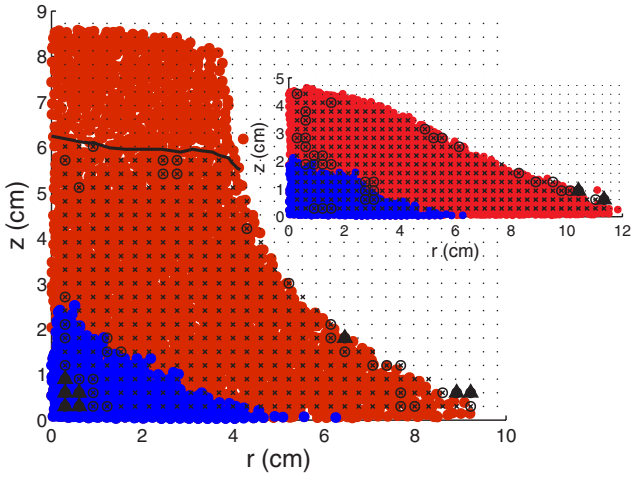

FIG. 4 (color online). The grid over which data was collected for $t = 0.14$ s and $a = 5$ (inset $t = 0.18$ s). Symbol positions indicate the centers of the $3d \times 3d$ averaging boxes and the type of symbol the misalignment angle ϕ between the principal axes of $\boldsymbol{\tau}$ and $\dot{\boldsymbol{\gamma}}^c$; $\phi < 5°$ crosses, $5° < \phi < 10°$ crosses with circles, and $\phi > 10°$ solid triangles. The pressure $P < 0.05 P_{\max}$ above the black line and the blue "stopped" region is defined by the threshold $|v| < 0.05|v|_{\max}$ where v is the speed.

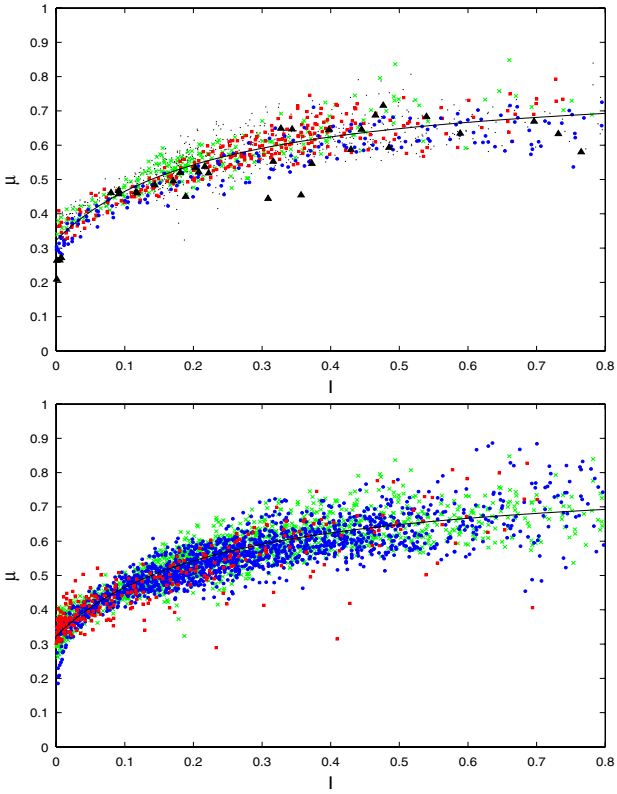

FIG. 5 (color online). μ against I for 3 different times at $a = 5$ (top: $t = 0.1$ s green crosses, $t = 0.18$ s red squares and $t = 0.26$ s blue dots with the remaining data at other times as small black dots; data with $\phi > 10°$ indicated by black triangles) and 3 different geometries (bottom: $a = 1$ red squares, $a = 5$ green crosses and $a = 8$ blue dots). The curve is the best fit line of the form (3) with $\mu_m = 0.5$. The maximum shear estimator for η is used here but the plot is essentially the same using the second invariant instead.

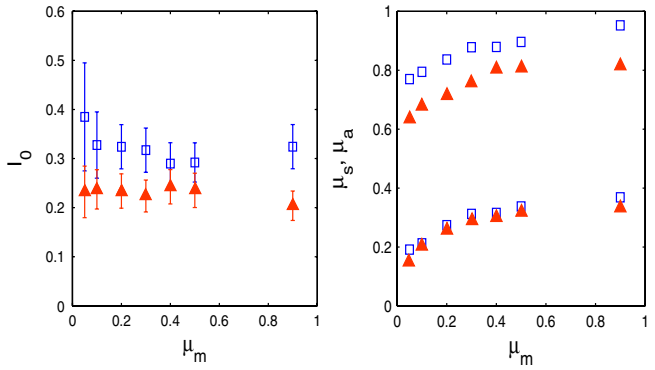

FIG. 6 (color online). The fitting parameters I_0 (left), μ_a (right, upper) and μ_s (right, lower) as a function of μ_m. Open squares from $|\tau|/|\dot{\gamma}^c|$ data and filled triangles from maximum shear data. Error bars are 95% confidence intervals (shown on the left, indicated by the size of symbol on the right).

misalignment was found near the boundary except at the rapidly moving head which is also close to the free surface.

Figure 5 shows how $\mu = \eta|\dot{\gamma}^c|/P$ varied with I for three different geometries and for three different times for the same geometry. The collapse onto a best fit line

$$\mu(I) = \mu_s + \frac{\mu_a - \mu_s}{I_0/I + 1} \tag{3}$$

as suggested by unidirectional flow experiments [3,7,21] is remarkable. There is clear evidence that not only is $\mu = \mu(I)$ but that the behavior for steady unidirectional flows carries over to unsteady, multidirectional flows. The theory is expected to fail in the jamming limit ($I \to 0$) but no indication of this breakdown is seen in the data. The functional dependence of the *macroscopic* friction μ, parametrized by (I_0, μ_s, μ_a), on the *microscopic* friction μ_m (see Fig. 6) is smooth and robust to whether $|\tau|/|\dot{\gamma}^c|$ or the maximum shear rate data is used. The values which emerge for the parameters are also reassuringly close to those found in experiments ([2]; $\mu_s \approx 0.4$, $\mu_a \approx 0.7$ and $I_0 \approx 0.3$) and fairly robust against changing the bottom roughness (the diameter of the glued-on particles was varied from a ratio of 0.5 to 4 times that of the flowing spheres).

The general applicability of viscoplastic theory found here is, frankly, a surprise given (a) the presence of a large growing static-flowing interface, (b) the proximity of most of the fast flow to the rough bottom boundary and (c) the existence of a large free surface. Certainly the misalignment between the principal axes of the local stress and strain rate tensors is most likely to be significant in these regions but still is never large ($<20°$ in the flowing regions). The major obstacle to a simple local rheology is, of course, nonlocal effects typified by the long range influence of boundaries. While this can be crucial for understanding steady flows [21], the extra presence of inertia in the momentum balance for transient flows appears to considerably reduce this influence.

The clear conclusion from this study is the ubiquity of the simple stress-strain rate relationship advocated by a simple viscoplastic continuum theory even in transient, multidirectional flow. Moreover, this relationship appears well fit with the experimental result for steady unidirectional flows and holds even near rough boundaries. This suggests that a simple viscoplastic modeling approach can be used to quantitatively capture granular flow properties (at least within $\pm 10\%$) in real geophysical and industrial applications.

The authors are grateful for helpful conversations with O. Pouliquen and J. Snoeijer, and thank E. Lajeunesse and H. Huppert for sharing their data. L. L. was supported by a Marie-Curie IntraEuropean fellowship.

*Laurent.Lacaze@imft.fr
†R.R.Kerswell@bristol.ac.uk

[1] H. M. Jaeger, S. R. Nagel, and R. P. Behringer, Rev. Mod. Phys. **68**, 1259 (1996).
[2] Y. Forterre and O. Pouliquen, Annu. Rev. Fluid Mech. **40**, 1 (2008).
[3] P. Jop, Y. Forterre, and O. Pouliquen, Nature (London) **441**, 727 (2006).
[4] I is a variant (square root) of a previously introduced Savage number [S. B. Savage and K. Hutter, J. Fluid Mech. **199**, 177 (1989)] and the Coulomb number [C. Ancey, P. Coussot, and P. Evesque, J. Rheol. (N.Y.) **43**, 1673 (1999)].
[5] F. da Cruz, S. Emam, M. Prochnow, J.-N. Roux, and F. Chevoir, Phys. Rev. E **72**, 021309 (2005).
[6] G. Lois, A. Lemaitre, and J. Carlson, Phys. Rev. E **72**, 051303 (2005).
[7] GDR MIDI, Eur. Phys. J. E **14**, 341 (2004).
[8] E. Lajeunesse, A. Mangeney-Castelnau, and J. P. Vilotte, Phys. Fluids **16**, 2371 (2004).
[9] G. Lube, H. E. Huppert, R. S. J. Sparks, and M. A. Hallworth, J. Fluid Mech. **508**, 175 (2004).
[10] N. J. Balmforth and R. R. Kerswell, J. Fluid Mech. **538**, 399 (2005).
[11] A. Mangeney-Castelnau, F. Bouchet, J. P. Vilotte, and E. Lajeunesse, J. Geophys. Res. **110**, B09 103 (2005).
[12] R. R. Kerswell, Phys. Fluids **17**, 057101 (2005).
[13] E. Larrieu, L. Staron, and E. J. Hinch, J. Fluid Mech. **554**, 259 (2006).
[14] L. Staron and E. J. Hinch, J. Fluid Mech. **545**, 1 (2005).
[15] L. Staron and E. J. Hinch, Granular Matter **9**, 205 (2007).
[16] R. Zenit, Phys. Fluids **17**, 031703 (2005).
[17] The commercially available software EDEM was used: http://www.dem-solutions.com.
[18] L. Lacaze, J. C. Phillips, and R. R. Kerswell, Phys. Fluids **20**, 063302 (2008).
[19] The volume fraction is typically in the interval [0.46, 0.62] but can decrease to 0.21 near a rapidly moving surface.
[20] I. Goldhirsch and C. Goldenberg, Eur. Phys. J. E **9**, 245 (2002).
[21] P. Jop, Y. Forterre, and O. Pouliquen, J. Fluid Mech. **541**, 167 (2005).